Classification of Bacterial Morphotypes from Images of ZN-stained Sputum-smears Towards Diagnosing Drug-resistant TB

Rijul Saurabh Soans
Dept. of Biomedical Engg.
M.I.T., Manipal University
Manipal, Karnataka, India.

A G Ramakrishnan
Dept. of Electrical Engg.
Indian Institute of Science
Bangalore, Karnataka, India.

V P Shenoy
Dept. of Microbiology
K.M.C., Manipal University
Manipal, Karnataka, India.

Ramesh R Galigekere
Dept. of Biomedical Engg.
M.I.T., Manipal University
Manipal, Karnataka, India

***Abstract*—We describe a method for identifying and classifying acid-fast bacilli (AFB) and their associated morphotypes in the microscope-images of Ziehl-Neelsen stained sputum smears, in the context of tuberculosis (TB) screening by image processing. The importance of our work stems from the fact that the transformation of the classical rod-shaped AFB into certain other shapes is said to be related to TB drug-resistance. The first stage of processing involves color-segmentation in the HSV space by using Neural Networks and RUS-Boosted Decision Trees. The latter is used to alleviate the effects of class-imbalance between the pixels belonging to the AFB and the background. The second stage involves categorizing the bacilli into regular rod-shaped ones (possibly beaded), their morphotypes ("V-shaped" or "Y-shaped" bacilli), and clumps. The main, and novel contribution in this paper involves identifying and classifying the bacterial morphotypes. For that purpose, we propose and investigate three different methods: The first involves assuming the morphotypes to be letters of the English alphabet, and using a letter-recognition technique based on the Hotelling Transform and the Discrete Cosine Transform on the color-segmented bacilli. The second method uses moment-based invariants on the silhouettes, boundaries and skeletons, respectively. We use Support Vector Machine and Weighted K-NN classifiers in both the cases. In addition, we describe a new method based on the ends of the skeleton. Experiments on 72 images of sputum-smears revealed that the skeleton-based approach performed better than the other methods.**

Keywords—TB, Drug resistant TB, TB morphotypes, Ziehl-Neelsen, Color pixel classification, RUS-Boost, SVM, Common/Difference Rates, Moment-based invariants, Skeletonization, Weighted K-NN classifier

I. INTRODUCTION

Tuberculosis (TB) is a highly infectious disease that affects the lungs or other parts of the body, and is a significant cause of death. In the recent past, drug-resistant TB forms – Multi-Drug resistant TB (MDR-TB) and Extensively-Drug resistant TB (XDR-TB) have been a major bottleneck in the progress made by TB-health care professionals. In 2014, an estimated 9.6 million TB cases were incident and 1.5 million people died from the disease. India alone accounts for about 2.2 million incident cases (2.2% MDR-TB) and 220,000 deaths [1].

Sputum smear microscopy – in particular, the low cost and highly-specific ZN-stained screening technique is still preferred in "high-burdened" countries to detect the presence of tubercle bacilli. In the recent times, *Xpert MTB/RIF* – an automated and non-invasive molecular diagnostic test is being adopted to detect MDR and XDR-TB. However, only 121 *Xpert MTB/RIF* equipped centers are currently operating in India [1], which is insufficient to serve the large volume of cases in the country. Consequently, sputum smear microscopy is still widely used towards speedy examination.

Several groups have worked extensively on automated detection of AFB in the context of ZN-stained sputum smear microscopy. A comprehensive literature review may be found in our previous work [2]. While many of them are limited to the detection of the classical rod-shaped AFB, [2] and [3] were the first to handle *beaded appearance* of tubercle bacilli. Note that the beaded appearance of AFB is due to changes in the levels of *Mycolic acid* present in the cell walls, and is linked to the virulence of the organism [4]. Another factor indicating the degree of virulence, is the presence of *clumps* (aggregates of bacilli that overlap or are close to each other), and were handled by the methods outlined in [2] and [5]; clumps occur due to the hydrophobic property of Mycobacterium tuberculosis [6]. More recently, our research group proposed a method of differentiating clumps and staining artefacts through texture-measures [7].

Typically, AFB are either rod-shaped (or slightly curved) with an average length and width of 4 μm and 0.4 μm, respectively [8]. Contrary to popular belief, variations in the shape of tubercle bacilli have been documented by Microbiologists, as early as in 1883 [9], [10]. However at that time, the claims were severely criticized and dismissed as 'Staining artefacts' [11]. Today, with the help of advanced imaging techniques such as Transmission Electron Microscopy (TEM) and Atomic Force Microscopy (AFM), it has come to be known that the tubercle bacilli do not always appear in the rod form [12]. In particular, [8] have shown the changes in the shape and size of AFB through TEM and AFM, and grouped them into various form factors including, "V-shaped", "Y-shaped", "Ultra-virus like" and "Spore-like" bacilli. Specifically, they report that the "V-shaped" bacilli occur due to *snapping post-fission* movements, wherein one or both the daughter cells abruptly swing around subsequent to the cell-division, thereby causing the distal arms to come closer while still remaining attached at the proximal end. Tubercle bacillus is also known to take on a "Y" shape with branches of greater length produced along its cylinder in XDR-TB [13]. Few people have actually

acknowledged the presence of these morphotypes in the context of automated detection of tubercle bacilli through light microscopy – [2] and [14] reported the presence of "V", "Y" and "T" shaped bacilli but did not categorize them explicitly, and the method in [15] labels them as 'Non-bacilli'. More recently, [16] reported on the morphological characterization of AFB, though based on Microscopic Observation Drug Susceptibility (MODS) assay – a culture method that takes about 7-10 days to obtain a result.

In this paper, we propose a method that not only identifies tubercle bacilli and counts them, but also that categorizes its morphotypes i.e. "V" or "Y" shaped bacilli. The benefits of such a method are two-fold: Automatic counting of AFB is useful to evaluate the grade of TB, and identification of morphotypes highlights possible drug-resistance. Our scheme involves color-pixel classification in the HSV space through a neural network. In addition, we recognize the problem of 'Class Imbalance' associated with the pixels belonging to the bacilli and the background, and alleviate the effects of the same by using Random Undersampling (RUS) Boosted Decision Trees. Subsequently, we use the methods [2] to handle beadedness and clumps. The results of colour segmentation and subsequent counting of AFB are evaluated and compared with the results in [2] through appropriate measures. Further, we propose and compare three different methods of identifying the TB-morphotypes. The first method involves the Hotelling Transform, followed by the retention of significant DCT coefficients as features. The next method utilizes moment-based invariants on the silhouettes, boundaries and skeletons of the binary version of bacterial morphotypes. In both the cases, we use SVM techniques and a weighted K-NN classifier to categorize the shapes. Finally, we propose a skeletonization of the aforementioned shapes followed by counting the number of end-points, to characterize the morphology of AFB. A flowchart of the methodology is provided in Fig. 1.

The rest of the paper is organized as follows: Section II describes color-pixel classification, and the subsequent procedures to handle beadedness and clumps. Section III describes categorization of bacterial morphotypes. Section IV presents the results of our methods on real data. Section V highlights the important contributions and future work.

II. Materials and Methods

A. The Dataset

The dataset comprises of images of size 1550 x 2088 (with a pixel size of 3.45 μm x 3.45 μm) captured from a Leica DFC 320 camera-attached microscope. The microscope has a 100x objective with a magnification of 10x for the lens. The images are standardized by keeping the exposure time, color saturation and gain fixed at 6.44 ms, 1.55x and 1.3x, respectively. We have used 36 images of smears associated with more than 12 patients to build our database for color-pixel classification. The results of color segmentation and counts of AFB, are generated on 20 separate images. Furthermore, we have acquired 72 new images with the aforementioned specifications, containing 72 "V-shaped" and 46 "Y-shaped" bacilli for the purpose of identifying and classifying TB morphotypes.

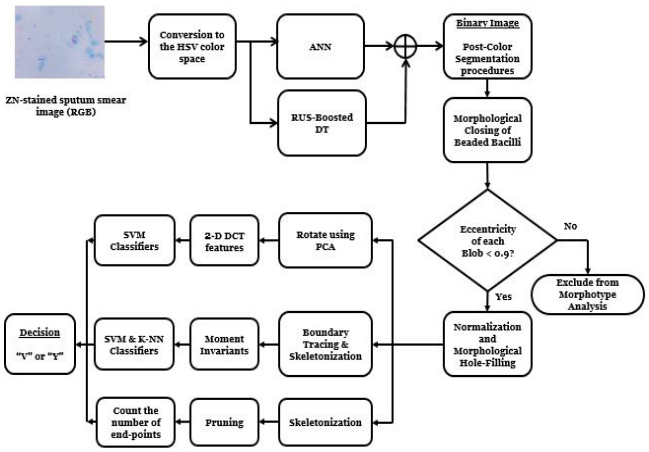

Fig. 1. Flowchart of the proposed methodology

B. Color-Pixel Classification

We perform color-segmentation in the HSV color space, since this model is close to the way humans perceive color. Moreover, the distribution of pixels (in terms of H, S and V) of the bacilli and those of the background were found to be fairly separate in this space. The HSV parameters can be obtained from RGB images through well-known formulae. Subsequently, we view the color segmentation of the candidate AFB as a non-linear binary classification problem and propose two methods for addressing the same:

1) Artificial Neural Networks (ANN): ANNs are particularly suited to handling non-linear classification problems, since they comprise various non-linear functions. Specifically, we use a supervised 1-hidden layer Back Propagation Network that utilizes the hyperbolic tangent function at all layers, and the Scaled Conjugate Gradient technique as the optimization criterion. The hyperbolic tangent function is chosen due to its asymmetric shape (useful for faster training) and its ability to output negative values (useful in data-normalization) [17].

2) Random Undersampling (RUS)-Boosted Decision Trees: RUS-Boost was first designed in [18] to handle 'Class Imbalance' *i.e.* when, in a training set, samples associated with one class greatly outnumber samples available in the other class(es). The logic behind the technique lies in the fact that the data points belonging to the minority class are most likely to be wrongly classified and consequently deserve greater chances of being selected for training in the following iterations. The data used in this paper happens to be a good example of class-imbalance. The training data set associated with the TB-Objects consists of ~50,000 pixels, whereas that of the background contains roughly 1 million pixels. This motivated us to perform boosting on Decision Trees, through resampling of the training set. Not surprisingly, RUS Boosted Decision Trees performed the best among all the other classifiers on our dataset.

We have also implemented the minimum Mahalanobis distance classifier and the Decision Trees in order to compare

the results with our prior work [2,7], which handle beadedness and clumps. We assess the efficacy of our color-pixel classification through Common/Difference Rates [19] after using the reference image created with the help of an experienced microbiologist.

C. Post-Color Segmentation Procedures

The output of the aforementioned color-pixel classifiers is a binary image consisting of many AFB regions including misclassified pixels (result of classification-error or debris). We use our criteria in [2] to reject noisy blobs (blobs with area ≤ 30 pixels). Moreover, in [2] we had proposed an algorithm, named as "Proximity Test" to handle Beadedness and "Proximity-Grouping" – a method using information on the proximity of parts of a bacillus, and area constraints – to categorize AFB into Individual, Beaded and Clumped Bacilli. We had specified the following ranges for area (in number of pixels): Individual Bacilli (say R_1) = [150, 900], Beaded Bacilli (R_2) = [400, 900], Clumps (R_3) = [>900]. However, we found R_1 = [150, 1120], R_2 = [350, 1120], R_3 = [>1120] to be more accurate. At this stage, we are able to produce the counts of AFB, useful in evaluating the grade of the disease. We use the measure "percent-correct" proposed by us in [2], to evaluate the efficacy of the algorithm in terms of AFB-counts.

III. Categorization of TB-Morphotypes

The classification of TB-Morphotypes into being "V-shaped" and "Y-shaped" bacilli is new, and forms a major contribution of this paper. We were able to identify 118 samples of Morphotypes – 72 "V-shaped" and 46 "Y-shaped" bacilli of which, we keep 50 of the former and 32 of the latter for training (70%), and the rest for testing (30%) purposes. We propose three methods for classifying the same, and compare them at the end.

A. A Handwriting Recognition Technique

The bacterial morphotypes resemble the English alphabets "V" and "Y", respectively. Consequently, one may exploit handwriting-recognition techniques to classify the morphotypes. First, the binary image, obtained after color-pixel classification, is subject to procedures outlined in Section II-C. The components of each of the beaded bacilli are clubbed together by morphological closing. Next, the blobs are subject to connected-component labeling and the Eccentricity for each blob is found. The method in [14] specified the lower-limit of Eccentricity for the classical rod-shaped AFB as 0.9. Hence, we exclude rod-shaped bacteria from further analysis by considering only those blobs having eccentricity below 0.9. Subsequently, the following steps are executed:

1) Find the bounding-box associated with each of the connected components (blobs). Rescale the blobs to fit a square box of size 32 x 32 – as suggested in [20] in an effort to produce the best classification. Bilinear interpolation is used for the purposes.

2) Perform Morphological 'hole-filling' to fill any possible holes in the rescaled binary image.

3) Apply the Hotelling Transform on the locations of the pixels in the 'letter' under consideration, to align them spatially in the direction of the principal-data-spread. The Hotelling Transform is given by:

$$y = A(x - m_x) \quad (1)$$

where y is the transformed data and A is the transformation matrix whose rows are the normalized eigenvectors of the Covariance matrix formed from the pixel locations of the morphotype. The data is mean-centered before transformation and the eigen-vectors are used to construct the principal-components transformation matrix.

4) Subsequently, use the Discrete Cosine Transformation (DCT) coefficients as features for classification of the 'character'. Specifically, [20] suggest to retain only 15% (roughly 154) of the DCT coefficients obtained through the zig-zag method used in the well-known JPEG compression technique [20].

5) Finally, store the features obtained from *Step 4* as training vectors for subsequent classification. Therefore, each morphotype is now represented by a 1 x 154 vector.

Steps 1-5 are performed for both the 'V' and the 'Y' shaped bacilli. The SVM classifier with a Linear Kernel (LK), Quadratic Kernel (QK), Radial Basis Function (RBF) Kernel and an inverse-squared Mahalanobis distance weighted K-NN classifier – are used for classification.

B. Moment-based Invariants

Moment-based invariants are well-established features for classifying objects in images. In this paper, we first follow *Steps 1-2* outlined in the preceding section to obtain the binary image (*Silhouette*) of the morphotype and store it for further processing. In addition, we trace the boundary of the blob using the Moore-Neighbor tracing algorithm modified by Jacob's stopping criteria [21]. Finally, we also extract the skeleton of each of the blobs [21], since it sufficiently represents the shapes "V" and "Y" under consideration. Subsequently, we compute moment-based features invariant to translation, rotation and scaling [22], on each of these three image sets to obtain the Silhouette Moments, Boundary Moments and the Skeleton Moments, respectively. These form the features for classification through the SVM-LK, SVM-QK, SVM-RBF and the weighted K-NN classifiers.

C. Skeleton-end-points

In this method, we use the topology of the morphotype as a distinguishing shape descriptor. We first follow *Steps 1-2* outlined in Section III-A, and then perform skeletonization [21] on the rescaled version of the morphotype. Note that, the skeleton may contain 'spurious' branches due to intra-variations in the shape of the morphotype. These branches can be *pruned* to reveal the underlying topology of the morphotype. The steps in the method are:

1) Skeletonize the rescaled version of the morphotype.

2) Locate the *end-points* and the *nodes* of the skeleton by counting the number of 8-connected neighbors for each point in the skeleton. The points along the skeleton have precisely 2 neighbors, and the *nodes* have more than 2 neighbors whereas the *end-points* have only one neighboring pixel.

3) Prune the spurious branches of the skeleton by starting at the *end-points* and removing touching pixels until a *node* is hit. In our case, we remove 6 touching pixels from the *end-points*. The value was found empirically for a size of 32 x 32.

4) Finally, locate and count the number of *end-points* in the pruned skeleton. If the number of *end-points* are 2, then the morphotype is classified as a "V-shaped" bacilli, and if the number of *end-points* are 3, then it is categorized as a "Y-shaped" bacilli. Morphotypes having more than 3 *end-points* are categorized as "Ambiguous" bacilli.

The method is based on the way humans identify the alphabets "V" and "Y" *i.e.* by counting the number of its end-points. Moreover, the method does not depend on the position or rotation of the morphotypes.

IV. Results

A. Color-Pixel Classification

Each pixel within a candidate AFB is characterized by 3 features *i.e.*, the values of *H, S,* and *V*. A pixel is classified as belonging to a bacillus or the background through Neural Networks and RUS-boosted Decision Trees. Note that, we have also used the Minimum Mahalanobis distance (MMD) classifier and Decision trees (DT), towards comparing the performance with our prior work [2,7]. All the classification models were optimized using the 10-fold cross-validation technique. A manual count of the AFB under the supervision of a microbiologist provided the ground truth for validation.

Two samples of ZN-stained sputum smear images and the corresponding results after color-pixel-classification, are shown in Fig. 2. The color-pixel classifiers are evaluated by the *Common & Difference Rates* (X-axis) as shown in Fig. 3. The Minimum Mahalanobis distance classifier had the lowest *Common Rate* (fewest number of pixels correctly identified). However, it did not produce too many false positives (low *Difference Rate*). The Neural network was better than the MMD and DT in terms of *Common Rate*, but produced a few false positives – as indicated by the *Difference Rate*. RUS-Boosted DT not only had the highest *Common Rate*, but also had the highest *Difference Rate* – an indication that it was very sensitive to any object similar in colour to AFB. Nevertheless, it had the highest *Delta-Rate* among the classifiers and therefore, is adjudged to be the best colour pixel classifier. Note that, we subsequently eliminate any noisy pixels as mentioned in Section II-C.

RUS-Boosted DT also performed the best in detecting AFB as shown in Table I using the *Percent-Correctness* formula introduced in [2]. A plot of the AFB counts, associated with different images, is shown in Fig. 4.

B. Categorization of TB-Morphotypes

Two samples of the "V-shaped" and the "Y-shaped" bacilli are shown in Fig. 5, along with their aligned-versions after having applied the Hotelling transform. Subsequently, methods mentioned in Section III-A and III-B are followed. The results are shown in Table II. The method based on moment-based invariants of the morphotype skeleton performed the best. A sample of "V-shaped" and "Y-shaped" bacilli along with their pruned skeletons are shown in Fig. 6. The counts of the morphotypes after counting the end-points of the pruned skeleton are shown in Table III.

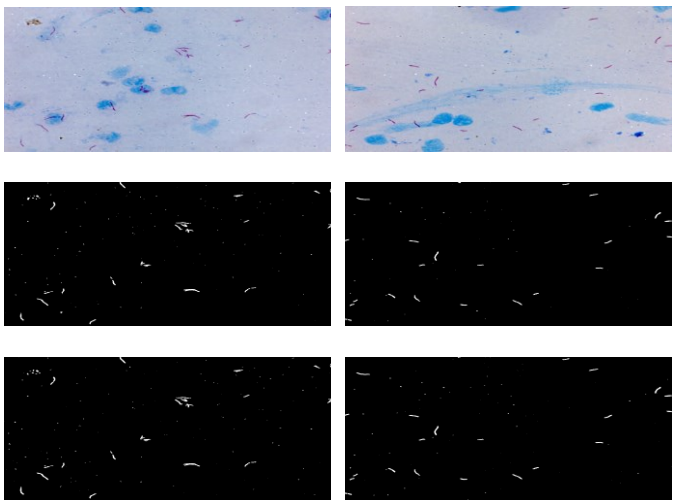

Fig. 2. (Top): The original images. (Middle): Color-pixel classification: Neural Network. (Bottom): Color-pixel classification: RUS-Boosted Decision Trees

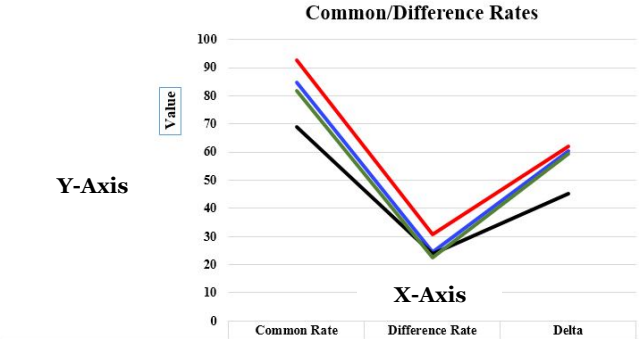

	Common Rate	Difference Rate	Delta
Neural Networks	84.7	24.3	60.4
RUS-Boosted Decision Trees	92.8	30.7	62.1
Minimum Mahalanobis Distance Classifier	68.9	23.7	45.2
Decision Trees	81.9	22.4	59.5

Fig. 3. Common/Difference Rate for different Color pixel classifiers

TABLE I. Percent-Correctness of the detection of AFB

Colour-Pixel Classifiers	AFB (Beaded and Unbeaded)	Beaded AFB
RUS-Boosted DT	96	92.3
Decision Trees	95.5	76.4
Neural Networks	93	72.2
MMD	81	92.8

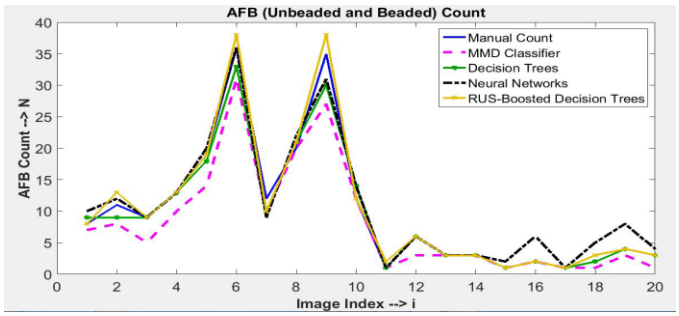

Fig. 4. AFB counts across different images.

TABLE II. PERFORMANCE OF THE CLASSIFIERS ON THE TB MORPHOTYPES

Features	CLASSIFIERS			Accuracy (%) Sensitivity (%) Specificity (%)
	Linear SVM	*Quadratic SVM*	*RBF-SVM*	*Weighted-KNN*
Handwriting Technique	**75** **66.6** **81.8**	60.8 51.2 65.8	65.8 68,4 65.3	NA[a]
Silhouette Moments	66.9 65.2 67.4	59.3 47.6 65.8	63.6 57.9 64.6	**73.7** **71.4** **74.7**
Boundary Moments	70.3 62.8 74.7	**80.5** **73.5** **85.5**	69.5 63.2 72.5	72.9 65.2 77.8
Skeleton Moments	76.3 72.5 78.2	**82.2** **80.5** **83.1**	**81.4** **90** **78.4**	78 76.3 78.8

[a] The covariance matrix associated with the Mahalanobis distance could not be inverted.

Fig. 5. (Left & Right): 2 samples of "V-shaped" and "Y-shaped" bacilli & their corresponding aligned versions after the Hotelling Transform.

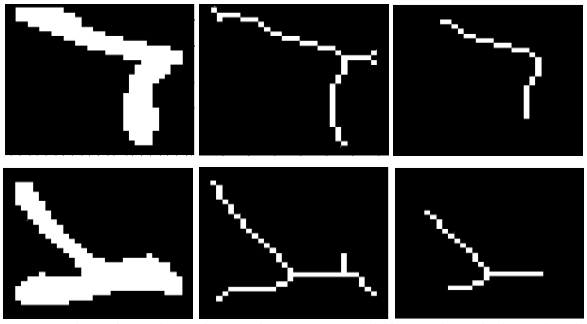

Fig. 6. (Left): The original morphotypes. (Middle): After skeletonization. (Right): After removing spurious branches

TABLE III. COUNTS OF TB-MORPHOTYPES USING METHOD III-C

TB-Morphotype	Manual Count	Computer Estimate	Accuracy (%)
V	72	68	94.4
Y	46	43	93.4

V. CONCLUSION AND FUTURE SCOPE

An automated algorithm has been developed to detect AFB and their associated morphotypes in images of ZN-sputum smears. The results of color-pixel classification and subsequent AFB counts, were compared and evaluated quantitatively. Subsequently, the morphotypes were handled using three different methods, and the method based on counting the ends of the skeleton gave the best results. In the future, we intend to work on images containing other morphotypes such as "Ultra-virus like" and "Spore-shaped" bacilli – which we have not encountered so far.

REFERENCES

[1] "WHO Global Tuberculosis Report 2015," (2015) [Online]. Available: http://apps.who.int/iris/bitstream/10665/191102/1/9789241565059_eng.pdf?ua=1

[2] R. Nayak, V. P. Shenoy, and R. R. Galigekere, "A new algorithm for automatic assessment of the degree of TB-infection using images of ZN-stained sputum smear," *Proc. Int. Conf. Systems in Medicine and Biology*, Kharagpur, pp. 294–299,2010.

[3] V. Makkapati, R. Agrawal, and R. Acharya, "Segmentation and classification of tuberculosis bacilli from ZN-stained sputum smear images," *Proc. IEEE Int. Conf. Autom. Sci. Eng.*, pp. 217–220, 2009.

[4] S. Malhotra, N. Bhatia, M. Kaushal, N. Kaur, and A. Chauhan, "Pleomorphic appearance in Mycobacterium tuberculosis," *J pub Heal. Epid*, vol. 2, pp. 11–12, 2010.

[5] Y. Zhai, Y. Liu, D. Zhou, and S. Liu, "Automatic identification of mycobacterium tuberculosis from ZN-stained sputum smear: Algorithm and system design," *Proc. IEEE Int. Conf. Robot. Biomimetics*, pp. 41–46, 2010.

[6] E. Julián, M. Roldán, A. Sánchez-Chardi, O. Astola, G. Agustí, and M. Luquin, "Microscopic cords, a virulence-related characteristic of Mycobacterium tuberculosis, are also present in nonpathogenic mycobacteria.," *J. Bacteriol.*, vol. 192, no. 7, pp. 1751–1760, Apr. 2010.

[7] R. S. Soans, V. P. Shenoy, and R. R. Galigekere, "Automatic Assessment of the Degree of TB-infection using Images of ZN-stained Sputum Smear: New Results," in *Proc. Int. Conf. Systems in Medicine and Biology*, Kharagpur, in press, 2016.

[8] A. A. V. and P. Farnia, *Understanding Tuberculosis - Deciphering the Secret Life of the Bacilli*. InTech, 2012.

[9] L. Malassez and W. Vignal, "The micro-organism of the Zoological tuberculosis (Sur le micro-organisme de la tuberculose zoogleique)," *Arch.Physiol.norm.path.,* vol. 3, no. 4, pp. 81–105, 1883.

[10] H. D. Vera and L. F. Rettger, "Morphological variation of the tubercle bacillus and certain recently isolated soil acid fasts, with emphasis on filtrability," *J. Bacteriol.*, vol. 39, pp. 659–687, 1940.

[11] K. R. Porter and D. Yegian, "Some Artifacts Encountered in Stained Preparations of Tubercle Bacilli: II. Much Granules and Beads.," *J. Bacteriol.*, vol. 50, no. 5, pp. 563–575, Nov. 1945.

[12] T. Ramakrishnan, P. S. Murthy, and K. Gopinathan, "Intermediary metabolism of mycobacteria," *Bacteriol Rev.*, vol. 36, pp. 65–108, 1972.

[13] A. A. Velayati, P. Farnia, M. A. Merza, G. K. Zhavnerko, P. Tabarsi, L. P. Titov, J. Ghanavei, M. Setare, N. N. Poleschuyk, P. Owlia, M. Sheikolslami, R. Ranjbar, and M. R. Masjedi, "New insight into extremely drug-resistant tuberculosis: using atomic force microscopy.," *Eur. Respir. J.*, vol. 36, no. 6, pp. 1490–1493, Dec. 2010.

[14] P. Sadaphal, J. Rao, G. W. Comstock, and M. F. Beg, "Image processing techniques for identifying Mycobacterium tuberculosis in Ziehl-Neelsen stains.," *Int. J. Tuberc. Lung Dis.*, vol. 12, no. 5, pp. 579–582, May 2008.

[15] R. Khutlang, S. Krishnan, A. Whitelaw, and T. S. Douglas, "Automated detection of tuberculosis in ZN-stained sputum smears using two one-class classifiers.," *J. Microsc.*, vol. 237, no. 1, pp. 96–102, Jan. 2010.

[16] A. Alva, F. Aquino, R. H. Gilman, C. Olivares, D. Requena, A. H. Gutiérrez, L. Caviedes, J. Coronel, S. Larson, P. Sheen, D. A. J. Moore, and M. Zimic, "Morphological characterization of Mycobacterium tuberculosis in a MODS culture for an automatic diagnostics through pattern recognition.," *PLoS One*, vol. 8, no. 12, pp. 1–11, Jan. 2013.

[17] K. Swingler, *Applying Neural Networks: A Practical Guide*. Morgan Kaufmann, 1996.

[18] C. Seiffert, T. M. Khoshgoftaar, J. Van Hulse, and A. Napolitano, "RUSBoost: A hybrid approach to alleviating class imbalance," *IEEE Trans. Syst. Man, Cybern*, vol. 40, no. 1, pp. 185–197, 2010.

[19] C. Meurie, G. Lebrun, O. Lezoray, and A. Elmoataz, "A comparison of supervised pixels-based color image segmentation methods.," *WSEAS Trans. Comput.*, vol. 2, no. 3, pp. 739–744, 2003.

[20] D. Kumar and A. G. Ramakrishnan, "Recognition of Kannada characters extracted from scene images," in *Proc. workshop on Document Analysis and Recognition - DAR '12*, Mumbai, pp. 15-22, 2012.

[21] R. Gonzalez. and R. Woods., *Digital Image Processing*, 3rd ed. Pearson Education Inc., 2009.

[22] Ming-Kuei Hu, "Visual pattern recognition by moment invariants," *IEEE Trans. Inf. Theory*, vol. 8, no. 2, pp. 179–187, Feb. 1962.